Supporting Information

Observation of a Transient Reaction Intermediate Illuminates the Mechanochemical Cycle of the AAA-ATPase p97

Simon Rydzek[1], Mikhail Shein[1], Pavlo Bielytskyi[1], Anne K. Schütz[1,2*]

[1]Bavarian NMR Center, Department of Chemistry, Technical University of Munich, 85748, Garching, Germany

[2]Institute of Structural Biology, Helmholtz Zentrum München, 85764, Neuherberg, Germany

* anne.schuetz@tum.de

Table of contents

Materials and Methods

Molecular biology, protein expression and purification

Reagents were purchased from Sigma-Aldrich if not otherwise indicated. DNA encoding human p97 protein with a hexa-histidine-tag and a TEV cleavage site attached to the N-terminus was obtained (Integrated DNA technologies). Point mutations were introduced via site-directed mutagenesis. All proteins were overexpressed in *Escherichia coli* BL21(DE3) cells in minimal M9 H_2O/D_2O (EURISOTOP) with $^{15}NH_4Cl$ and [^{1}H,^{13}C] /[^{2}H,^{12}C]-glucose as the sole nitrogen and carbon sources for solid/solution-state NMR, respectively. Selective labelling with I-δ_1-[$^{13}CH_3$], V/L-γ_1/δ_1(*proR*)-[$^{13}CH_3$,$^{12}CD_3$] (Sigma/NMR-bio) and M-ε_1[$^{13}CH_3$] (Cambridge Isotope) and protein purification were achieved as described before[1].

NMR sample preparation

Samples for solution-state NMR were exchanged via dialysis or ultra-filtration into the respective D_2O buffers at protein concentrations between 200-300 μM. For apo state, ATPγS-bound state (5 mM ATPγS

Jena Bioscience, 4 mM $MgCl_2$) and the regeneration system, the buffer contained 25 mM HEPES pH 7.5, 25 mM NaCl, 5 mM TCEP; for ADP-bound state (10 mM ADP), the buffer contained 25 mM HEPES pH 7.0, 50 mM NaCl, 5 mM TCEP. Salts (magnesium, vanadate, arsenate) and nucleotides as well as components of the regeneration system indicated below were added as stock solution ranging from 100 mM to 1 M in NMR buffer. Solution-state NMR was performed in 3 mm tubes and Shigemi tubes. For solid-state NMR, the protein was sedimented into 1.3 mm outer diameter Bruker rotors (Cortecnet) using a Beckmann ultracentrifuge (SW32 rotor) and commercial filling tools (Giotto Biotech).

Setup of the ATP regeneration system and phosphate mimics

For the ATP regeneration system, the following ingredients were added: 4 mM $MgCl_2$, 50 mM KCl, 4 mM ribose-5-phosphate, 150 mM PEP for E305Q mutants and 200 mM PEP for all other measurements, 20/40 units pyruvate kinase from *Bacillus stearothermophilus* for 150/300 µL reaction volumes and finally 10 mM ATP. The concentrations of p97 were 200 µM for R95G, L198W and R155H mutants and 300 µM for all others. Vanadate $(VO_4^3)^-$ and arsenate (AsO_4^{3-}) were added from stock solutions of 500 mM. Arsenate stock solution was prepared from sodium arsenate directly in NMR buffer, whereas vanadate stock solution was prepared as described in the manufacturer's manual for sodium orthovanadate (Sigma). For measurements of p97 under ATP turnover with arsenate and vanadate as modulators, the respective stock solution was added together with the components of the ATP regeneration system, right after addition of $MgCl_2$ before ATP was added. Measurements of vanadate and arsenate binding to the ADP-bound state of p97 were performed in the same buffer as for the regeneration system at a reduced protein concentration of 50 µM. The phosphate-mimicking ions (50 mM) and 4 mM $MgCl_2$ were added before 10 mM ADP was added. For solid-state NMR, samples with ATP regeneration system were prepared in H_2O buffer with 5 mg of protein in a final volume of 500 µL, which was sedimented into the NMR rotor. Concentrations of PEP and pyruvate kinase from rabbit muscle were adjusted to 50 mM and 67 units.

NMR data acquisition and analysis

Solution-state NMR experiments were recorded at Bruker spectrometers operating at field strengths corresponding to proton resonance frequencies of 800, 900 and 950 MHz at 50 °C sample temperature. Solid-state NMR experiments were recorded at a Bruker spectrometer at a field strength corresponding to a proton resonance frequency of 800 MHz and sample temperatures of 7 °C and 20 °C, determined from the water frequency with respect to DSS. The 1.3 mm Bruker probe was operated in ^1H, ^{13}C, ^{31}P triple resonance mode at a MAS rate of 45 kHz. Spectra were processed using Topspin and analysed using CcpNMR[2]. The solid-state NMR spectra were referenced to DSS. Experimental parameters are listed in Tables S4 and S5. All other data analysis was accomplished via home-written MATLAB and Origin scripts. Visualizations of protein and nucleotide structure were accomplished in Pymol version 2.3[3-5].

Quantification of kinetics

To monitor concentrations of ATP, ADP and PEP in the reaction mixture over time, respective regions in one-dimensional ^1H NMR spectra were integrated in Topspin. The regions used for integration are displayed in Figure S2. For PEP the integral obtained in the first spectrum recorded was set to 100%. To obtain relative concentrations of the nucleotides, the sum of ATP and ADP integrals was taken as 100%. For all data points, an error of 5% originating from the integration procedure and spectral noise is estimated. The ^{31}P-spectra were analysed in a similar way using the signals depicted in Figure S6a.

ATPase activities were calculated as initial rates from the derivative with respect to time of the PEP concentration either utilizing a linear fit or in case of fast reacting mutants by taking the slope of the non-linear fit. Errors were either obtained from standard deviation of the linear fit or, if the error from standard deviation was lower than 10%, set to 10% as the minimal error based on inaccuracy of the

protein concentration determination. For cases where the initial slope was used, the error was set to 15% as this method is more prone to inaccuracies from the non-linear fit.

Simulations of nucleotide occupancies

Nucleotide concentrations were determined as mean values in five regions (I-V in Figure 1b) of the ATPase reaction, obtained via integration of ^{1}H NMR spectra as described above. The analysis was extended to ten commensurate regions, each comprising 5-6 interleaved two-dimensional spectra, where extensive coverage of different nucleotide ratios was required. ATPase activities were determined as described above but additionally the decrease of ATP levels was taken into account, which becomes significant upon depletion of PEP (starting in region III of Figure 1b). The very good correlation between the overall ATPase activity of the reaction system and the proportion of p97 in ADP.P_i state is shown in Figure 4a. Hence, the post-hydrolysis product, or ADP.P_i state, was taken as a proxy for prior ATP binding. The proportions of ADP.P_i state versus ADP state of p97 were determined from integration of HMQC peaks of residue I206 (Figure 1d). The assumption that throughout the ATPase reaction all p97 subunits are occupied by either ADP or ADP.P_i is justified for the following reasons: (*i*) The NMR spectra at all time points can be fully explained by a mixture of ADP and ADP.P_i states. (*ii*) The abundance of ATP-bound p97 is estimated below 3% from the signal intensities determined at the positions of correlations that are characteristic of the up-state of NTD. (*iii*) Given nucleotide affinities in the nanomolar range and a 33-fold excess of nucleotide over p97 monomers in solution, significant amounts of apo state can be safely excluded.

The overall uncertainty of all quantities derived from measured values (*i.e.* concentrations of free nucleotides, populations of protein nucleotide states and ATPase activities) was calculated from individual uncertainties *via* formula [S1] for uncertainty propagation:

$$\Delta y = \sqrt{\sum_i \left(\frac{\partial y}{\partial x_i} \cdot \Delta x_i\right)^2} \qquad [S1]$$

In order to rationalize nucleotide binding in the presence of ATP/ADP mixtures, different models of inter-subunit coordination were implemented. To compare the models while taking into account the respective number of fitted parameters, two different values were used: (*i*) the adjusted R^2-value obtained from MATLAB, whereby values closer to one represent better fits, and (*ii*) the corrected Akaike Information Criterion (AICc). Here, n is the sample size (n = 10, with experimental values from ten regions of the ATPase reaction), *SSE* is the sum of squares due to error from MATLAB, and K is the number of fitted parameters. The AICc is calculated according to formula[6] [S2]:

$$\mathrm{AICc} = n \cdot \log\left(\frac{\mathrm{SSE}}{n}\right) + 2 \cdot K + \frac{2 \cdot K \cdot (K+1)}{n-K-1} \qquad [S2]$$

The AICc values and fitted parameters of the best performing models are summarized in Table S3.

Model 1: Different affinities for ATP and ADP

The probability p of binding one molecule of ADP to one nucleotide binding site in the absence of cooperativity was calculated according to formula[7] [S3] with K_d values adapted from the literature[8]:

$$p_{ADP} = \frac{[ADP] \cdot K_{d,ATP}}{K_{d,ATP}K_{d,ADP} + [ATP] \cdot K_{d,ADP} + [ADP] \cdot K_{d,ATP}} \qquad [S3]$$

K_d values of ATP and ADP binding to p97-ND1L obtained by SPR[8] were considered because ITC-based values[9] were limited to ATPγS. Taking error margins into account, the experiment predicts 1.0-1.6 fold tighter binding of ADP over ATP (Figure S14a). In contrast, only 30-fold tighter binding of ADP over

ATP could explain the proportion of p97 detected in ADP state over the full range of ATP/ADP ratios investigated (Figure S14b).

Model 2: Cooperative ADP binding according to Hill
A plot was made according to the Hill equation[10] with θ as the fraction of protein bound to the respective nucleotide [S4]

$$log\left(\frac{\theta}{1-\theta}\right) = n_H \cdot log([Nucleotide]) - log\left(K_{\mathrm{d,Nucleotide}}\right) \quad [S4]$$

A high Hill coefficient n_H would indicate strongly cooperative binding of ADP. The Hill plot (data not shown) did not show good adherence to the experimental data, presumably due to competition of two ligands binding to two distinct protein conformations. K_d-values derived from abscissa intersections (≈400 μM for ADP and ≈10 mM for ATP) were not consistent with literature values[8, 11, 12] and hence the obtained n_H (1.8 for ADP and 6.1 for ATP) were not meaningful. The Hill model was not considered further.

Model 3: Concerted conformational transitions according to Monod-Wyman-Changeux
The Monod-Wyman-Changeux (MWC) model describes concerted transitions in multimeric proteins made from identical subunits[13]. It considers two states, the relaxed state (R-state) and tense state (T-state). All subunits must be in the same state. Binding of a ligand to the T-state, which has a higher initial population, results in a transition to the R-state, which has a higher affinity for the ligand. The relevant parameters for this model are L - the ratio of equilibrium concentrations of T-state to R-state in the absence of ligand; c - the ratio of K_d-values for the ligand of R-state to T-state; α - the ratio of free ligand concentration to $K_{d,R}$; n - the number of subunits with a binding site per protein multimer.
The T-state was equated with the up-state of NTD, found in apo or ATP-bound p97 alike, and the R-state with the down-state, found in ADP-bound p97. The population of R-state, $\bar{R}$, was then calculated according to formula [S5]:

$$\bar{R} = \frac{(1+\alpha)^n}{(1+\alpha)^n + L\cdot(1+c\cdot\alpha)^n} \quad [S5]$$

The best fit of this model is shown in Figure S14d and the fitted parameters are listed in Table S3. Since in the absence of ADP (apo state, Figure 1c), the T-state alone is observed in NMR spectra, $L > 10^5$ is consistent with the experiment. However, the fitted value of $K_{d,R}$ is two orders of magnitude higher than the experimental value[8] of $K_{d,ADP}$ = 100 nM.

In the standard MWC model, only the binding of one ligand to p97 is considered. A more sophisticated form of the MWC model was implemented. ATP is introduced as a competitive ligand for ADP with a potentially higher affinity for the T-state. Including $\bar{\alpha}$ - the ratio of free concentration of a competitive ligand to its $K_{d,R}$ and $\bar{c}$ - the ratio of K_d-values for the competitive ligand of the R-state to T-state, formula [S6] was derived[14]:

$$\bar{R} = \frac{(1+\alpha+\bar{\alpha})^n}{(1+\alpha+\bar{\alpha})^n + L\cdot(1+c\cdot\alpha+\bar{c}\cdot\bar{\alpha})^n} \quad [S6]$$

With this generalized MWC model, the fitted value of $K_{d,R}$ for ADP is close to the experimental value but the fitted value of $K_{d,T}$ for ATP is still two orders of magnitude higher than the experimental value. The best fit of this model is shown in Figure 4b. Although the fits for both MWC models are similar (Figures 4b, S14d), due to the increased number of fitted parameters, the goodness of fit according to adjusted R^2- and AICc-values is lower for the MWC model including competitive binding. The fitting parameters are summarized in Table S3.

Model 4: Probabilistic model

The probabilistic model considers independent nucleotide binding events to the six sites within one hexamer[7, 15]. The probability p of binding ADP to one binding site in the absence of cooperativity was calculated according to formula [S3]. In order to determine the probability P of a minimum of n ADP per hexamer, a binominal distribution was calculated according to formula [S7]:

$$P = \sum_{i=n}^{6} \binom{6}{i} p^i (1-p)^{6-i} \qquad [S7]$$

Probability curves over the nucleotide concentration range present in the experiment were obtained and compared to the observed nucleotide occupancies. A minimum of n = 1 ADP molecules to enforce an all-ADP-bound p97 hexamer and twofold tighter binding of ADP over ATP fitted the data best and is shown in Figure S14c. The fitted affinities are close to the experimental ones for both ATP and ADP and are summarized in Table S3.

Calculations of kinetic parameters of the reaction cycle

The model shown in Figure 4c can be summarized as

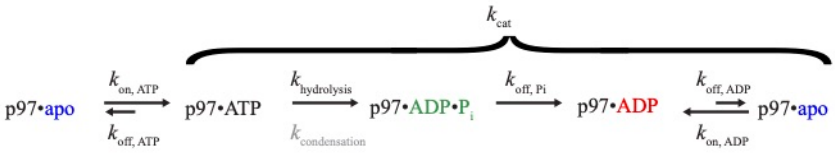

For this reaction scheme, a steady-state turnover rate k_{cat} at saturating ATP levels has been derived according to Michaelis-Menten kinetics[16]. If steps following phosphate release are more rapid than steps preceding, the turnover rate is given by [S8]

$$k_{cat} = \frac{k_{hydrolysis} \cdot k_{off,Pi}}{k_{condensation} + k_{off,Pi} + k_{hydrolysis}} \qquad [S8]$$

If hydrolysis is irreversible, it simplifies to

$$k_{cat} = \frac{k_{hydrolysis} \cdot k_{off,Pi}}{k_{off,Pi} + k_{hydrolysis}} \qquad [S9]$$

From [S9], it follows that either hydrolysis or phosphate release determine k_{cat}, whichever is smaller, $k_{hydrolysis}$ or $k_{off,Pi}$.

The kinetic rate constants of the reaction cycle model from Figure 4c are summarized in Table 1 and were inferred based on the following arguments:

(*i*) ATP-, ADP.P$_i$- and ADP-bound p97 could be observed by protein-detected NMR under ATP turnover and their populations quantified. Therefore, the rate-limiting step can be deduced from the predominant p97 species in the NMR spectra. This step determines the overall apparent k_{cat}, which is the ATPase activity in the presence of saturating ATP levels (Figures 3a, S11). Therefore, values for either $k_{off,Pi}$ or $k_{hydrolysis}$ were equated to k_{cat}: the locked, or ADP.P$_i$ state, is predominant for wild-type p97 ($k_{cat} \sim k_{off,Pi}$) while for disease mutants with E305Q mutation, it is the pre-hydrolysis state ($k_{cat} \sim k_{hydrolysis}$).

(*ii*) The nucleotide on- and off-rates ($k_{on/off,ATP}$ and $k_{on/off,ADP}$) were obtained by SPR[8], transferred to the nucleotide concentration in the reaction system (10 mM), and adjusted to match the experimental temperature of 50° C. To this end, activation energies of nucleotide binding and release in the range of 30-60 kJ/mol were assumed, adapted from values for the actomyosin V/VI ATPase[17, 18]. According to the Arrhenius equation, this translates into three- to tenfold acceleration of binding and release events between 20°C and 50°C. Similar affinities and nucleotide on-/off-rates for D1 domain within p97-ND1L and the full-length construct were reported[8, 11]. We note that these values were determined in the

presence of pure ADP/ATP, not nucleotide mixtures. The apparent K_d-values in the presence of nucleotide mixtures can differ. The on-rates are much faster than all other kinetic parameters, hence the apo state is never observed. The off-rates are faster than overall k_{cat} but not by several orders of magnitude.

(*iii*) For disease mutants without mutation in the Walker B motif, no single rate-limiting step could be determined as the NMR spectra showed a mixture of nucleotide states from the very beginning, due to the rapid progression of the ATPase reaction with respect to the time scale of the NMR experiments. Therefore, the relative speed of nucleotide hydrolysis, phosphate and ADP release could not be quantified with certainty and all these steps could potentially contribute to limit the reaction speed. As ADP was already present in solution during the acquisition of the first methyl spectrum, ADP-bound p97 was inevitably detected. Yet it cannot be safely excluded that $k_{off,ADP}$ also contributes to limit the overall reaction cycle. The estimates of kinetic parameters summarized in Table 1 reflect this possibility.

(*iv*) Glutamate E305 in the Walker B motif D1 domain is generally assumed to activate the water molecule for ATP hydrolysis[19]. Therefore, the E305Q mutation is frequently employed to slow down ATP hydrolysis. Yet it cannot be excluded that this mutation also alters the kinetic rates of subsequent steps. In particular, the removal of a negative charge from the binding pocket could slow down the ejection of the negatively charged phosphate ion. As the protein-detected NMR spectra recorded on wild-type and E305Q p97-ND1L show the same transient reaction intermediate, the E305Q mutation clearly does not change the rate-limiting step of the reaction cycle. Rather, it must slow down both ATP hydrolysis and phosphate release and this is reflected in the kinetic rate constants in Table 1. An alternative explanation would be that ATP hydrolysis is rate limiting already in the wild-type protein and therefore, the E305Q mutation has no further effect. However, this interpretation contradicts firstly the protein-detected NMR spectra, which indicate that the NTD assumes the down state in the reaction intermediate, similar to ADP- but not ATPγS-bound p97, and secondly the nucleotide-observed NMR spectra, which establish that the nucleotide is caught post hydrolysis in the reaction intermediate.

Supporting Figures

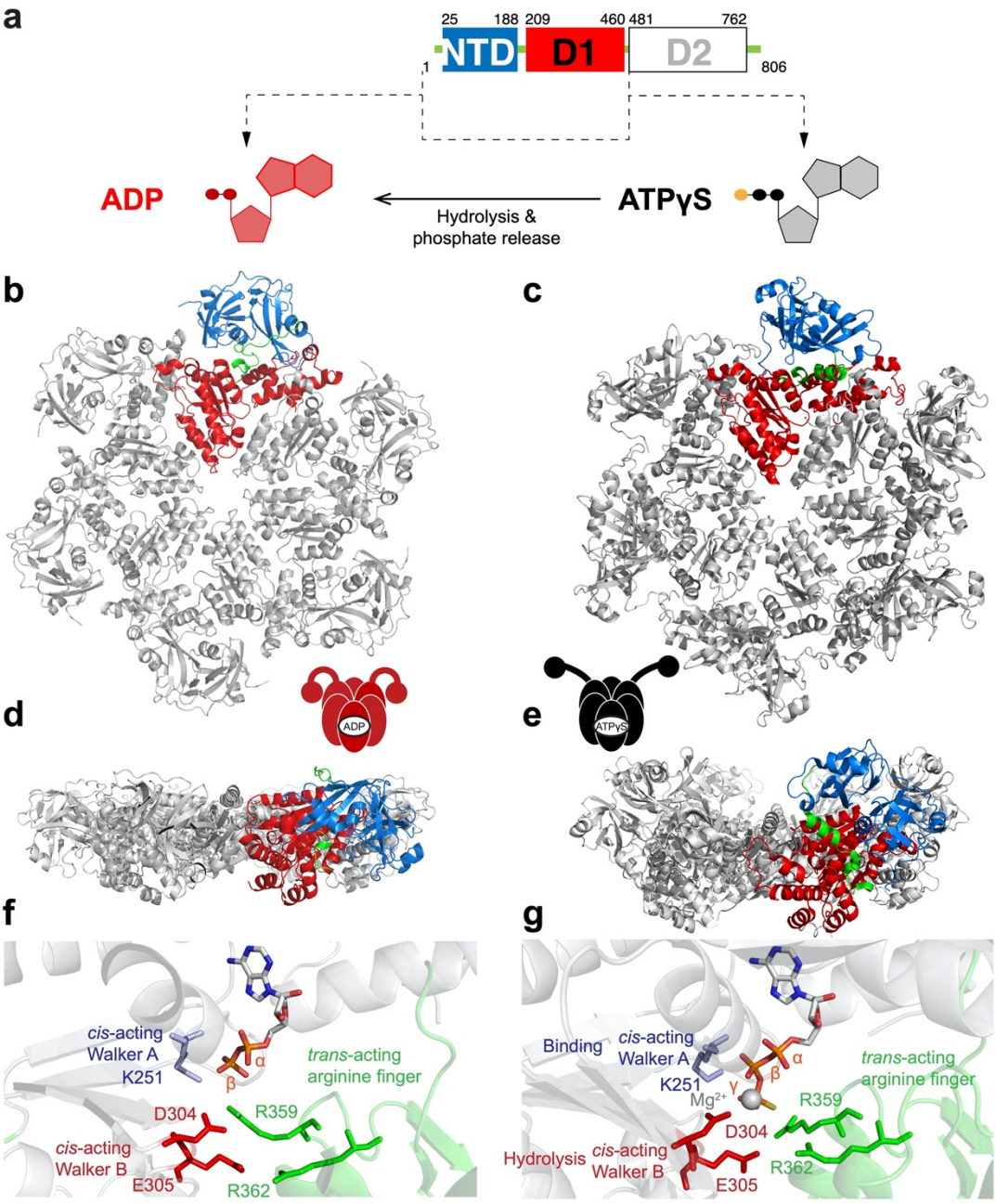

Figure S1. Static nucleotide states of p97. a. The p97 domains with colour coding from N- to C-terminal: N-terminal domain (NTD, blue) followed by two nucleotide binding domains D1 (red) and D2 (white). **b, c** Top and **d, e** side views of structures of p97-ND1L trapped at defined points in the ATPase cycle, solved by Xray crystallography: ADP-bound (PDB: 1e32) and ATPγS-bound (with R155H mutation PDB: 4ko8). The type of nucleotide bound in D1 dictates the position of the NTD (blue) with respect to the hexamer formed by D1 as well as the conformation of the N-D1 linker (green), while the D1 domain (red) remains mostly unaltered. **f, g** Focus on the nucleotide binding pocket in D1: Walker A residue K251 promotes nucleotide binding, Walker B residues E305 and D304 initiate hydrolysis and *trans*-acting arginine fingers R359 and R362 stabilize the nucleotide of the adjacent protomer. These residues are shown as sticks, the magnesium ion bound to ATPγS as a grey sphere.

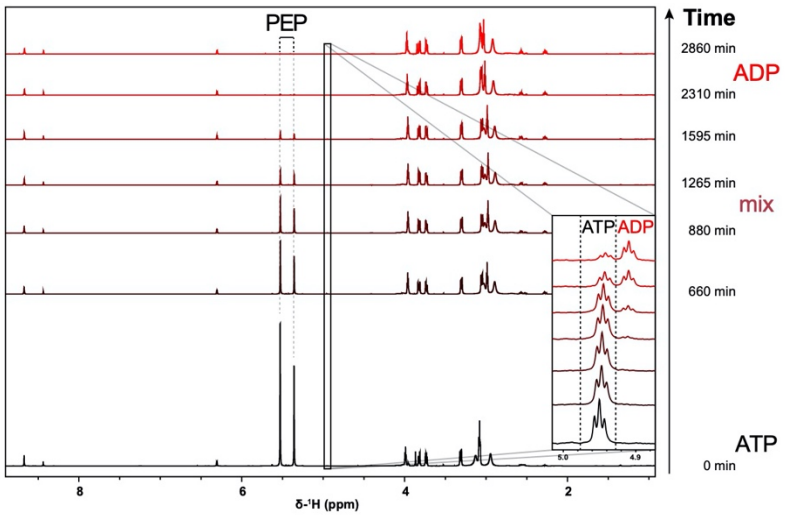

Figure S2. Time course of the ATPase reaction of p97-ND1L in solution. Time course of 1D ^{1}H NMR spectra recorded interleaved with 2D HMQC spectra during the reaction of p97-ND1L wild type with the regeneration system. The corresponding regions I-V are indicated in Figures 1b and S4a. Spectra were chosen at time points denoted on the right representing the beginning of the reaction (0 min), the middle of regions II-IV (660-1265 min) and three stages of nucleotide mixtures from region V (1595-2860 min). The signals of PEP, ATP and ADP that were integrated for quantification are labelled. The signals of the nucleotides used for integration were chosen such that they provided the clearest separation.

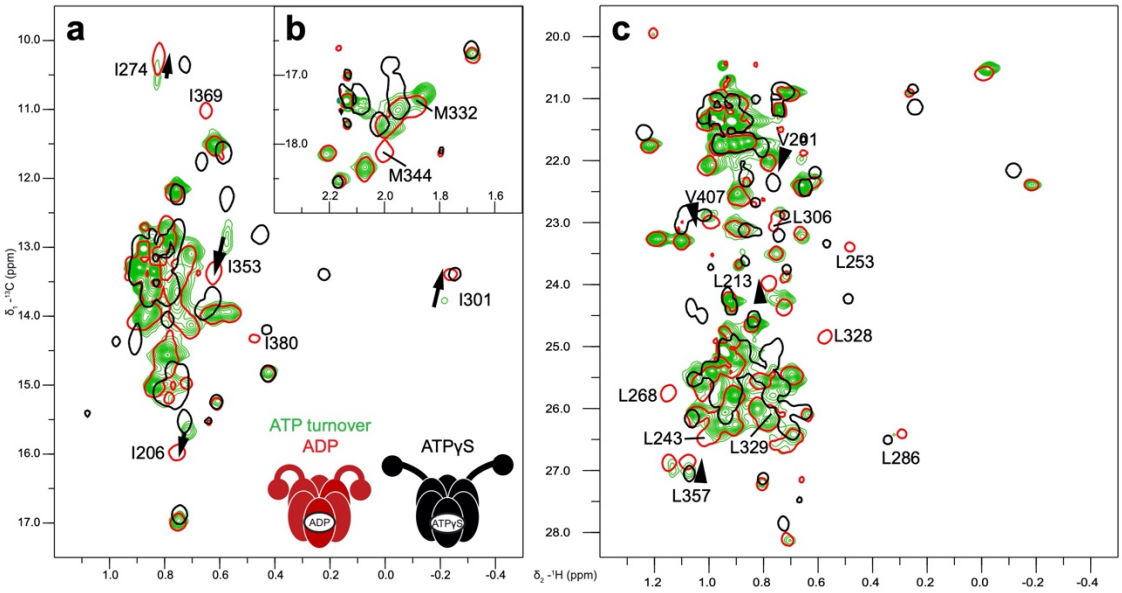

Figure S3. Complete methyl spectra of p97-ND1L recorded during ATP turnover. Superposition of HMQC spectra of ILVM *proR*-$^{13}CH_3$-labelled p97-ND1L wild type in the presence of pure ATP (green contours, corresponding to region I in Figures 1b and S4a) with ATPγS- (black) and ADP-bound (red) reference spectra as single contours. The full spectrum is divided in regions that contain **a** isoleucine, **b** methionine and **c** leucine and valine residues. Residues that show chemical shifts perturbations between spectra recorded at the beginning of the ATPase reaction (in the presence of ATP) and towards the end of the reaction (predominantly ADP) are highlighted. Arrows indicate the corresponding peak movements during the course of the reaction.

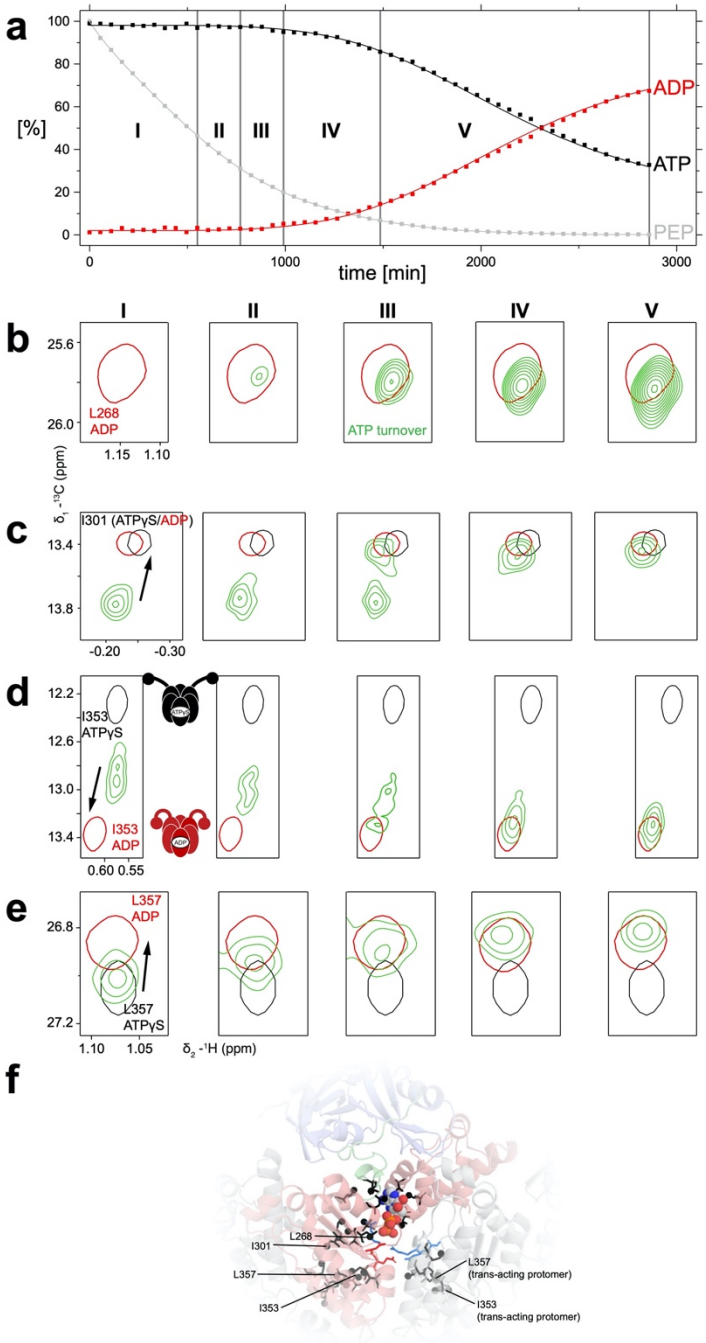

Figure S4. ATPase reaction of p97-ND1L monitored in real time. a. Time course of nucleotide turnover by p97-ND1L in the presence of the ATP regeneration system. Squares represent recorded data and lines indicate fitted values. Relative abundance of ATP, ADP and PEP were quantified by integration of respective regions in ^{1}H 1D NMR spectra (Figure S2). ATP turnover is inhibited in the presence of ADP. As it would take very long for all ATP to react, the experiment was terminated before completion of the reaction. **b-e.** Time course of HMQC correlations from different residues throughout the reaction. The spectra shown were obtained from 45-minute individual spectra, which were summed up into five blocks as indicated in panel a. This allowed us to observe changes in a time-resolved manner. Upon depletion of PEP, as ADP levels built up in the reaction system, the entire spectrum reverted to the ADP-bound reference. Remaining minor chemical shift perturbations were attributed to the absence of components in the reference samples, e.g. 200 mM pyruvate and phosphate and 50 mM KCl. **f.** Location of the residues of interest on the crystal structure (ADP-bound p97-ND1L, PDB: 1e32).

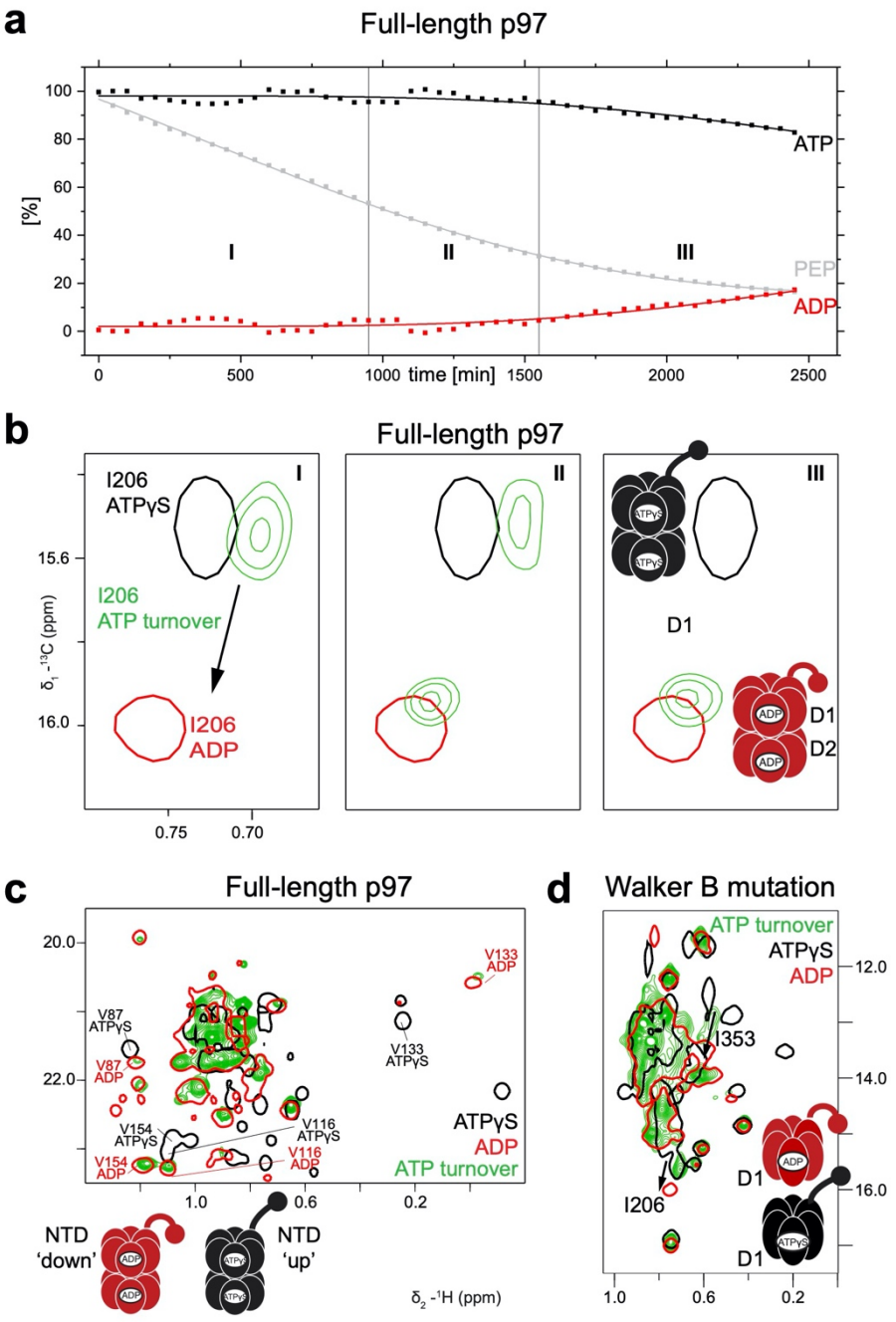

Figure S5. ATPase reaction of full-length p97 and the Walker B motif mutant. a. Nucleotide and PEP turnover during the reaction of full-length p97 with the ATP regeneration system. Concentrations were quantified from the respective resonances in ^{1}H 1D NMR spectra. **b.** Closeup of the methyl correlations of residue I206 in full-length p97 during ATP turnover for regions I-III from panel a. Analogous observations were made to p97-ND1L in Figure 1d: The correlation (green) starts from an ATPγS-like position (black). As ADP levels build up, it doubles and appears at the same position as the ADP-bound reference (red). **c.** Valine region of spectra recorded on full-length p97 during ATP turnover, summed up in region I. The spectrum shows overall similarity to the reference spectrum of ADP-bound full-length p97. Some weak correlations are reduced in intensity beyond detection at the signal-to-noise level achievable in the presence of the regeneration system. **d.** Superposition of p97-ND1L E305Q during ATP turnover (green) with ATPγS- (black) and ADP-bound (red) reference spectra in the isoleucine region. Again, similar observations to region I of the corresponding spectra of p97-ND1L without Walker B mutation were made (Figures 1d and S3a).

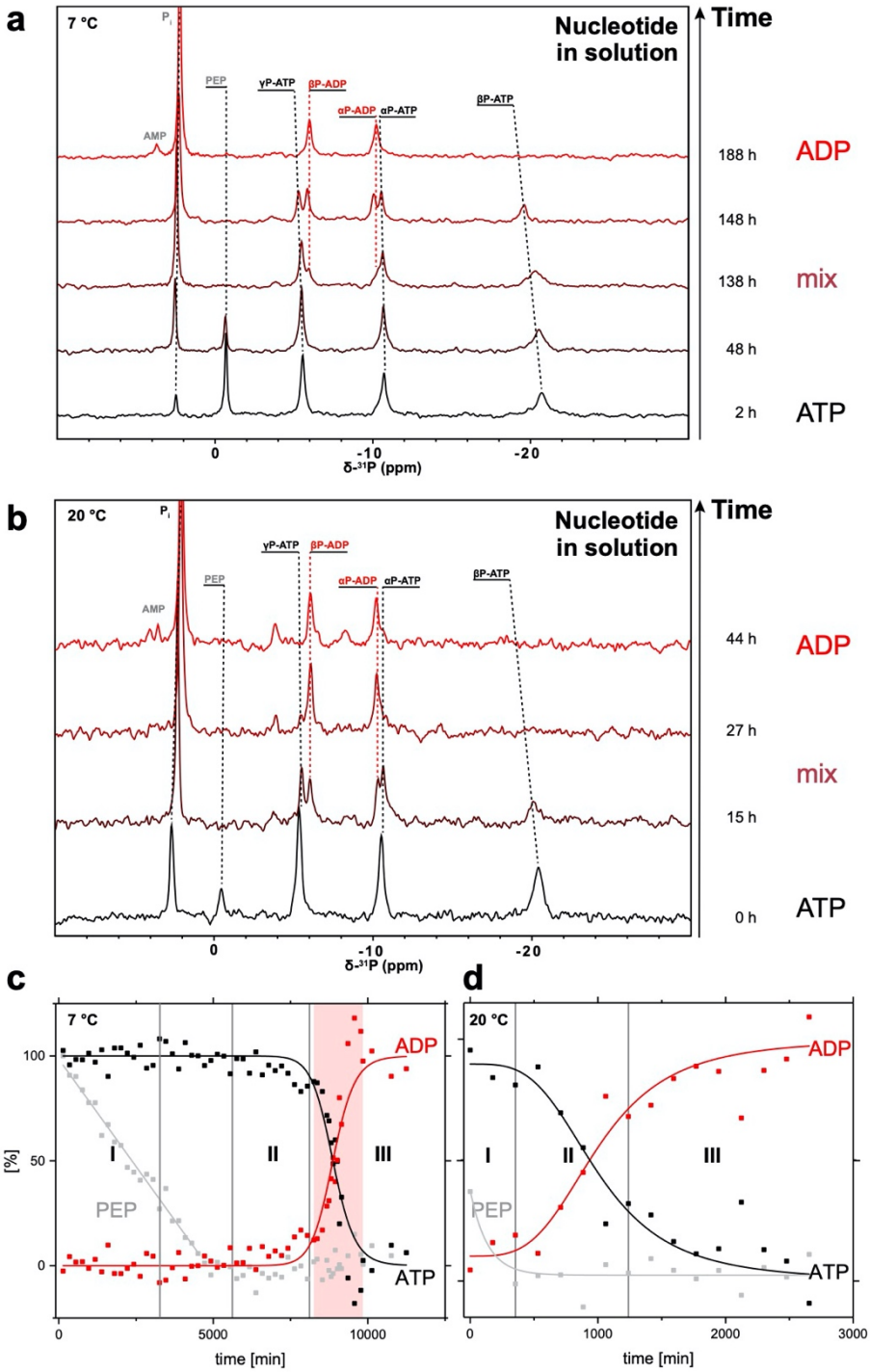

Figure S6. Time course of the ATPase reaction of p97-ND1L in the sediment. Directly pulsed ^{31}P one-dimensional NMR spectra were acquired to follow the kinetics of nucleotide turnover by p97-ND1L E305Q in the sediment at 7 °C (**a**) and 20 °C (**b**). Relative abundance of ATP, ADP and PEP were quantified by respective phosphate resonances: PEP: -0.7 ppm; β-ATP: -20.0–20.7 ppm; ADP concentration by subtracting the ATP fraction from 100%. The results are plotted in panel **c** for 7 °C and **d** for 20 °C. Cross-polarization spectra, which were acquired in an interleaved manner with the directly pulsed experiments, were summed up separately for regions I-III and are shown in Figure S7. In order to speed up reaction for the 7 °C time series, temperature was increased to 30 °C during the period highlighted in red in panel c, and afterwards again decreased to 7 °C.

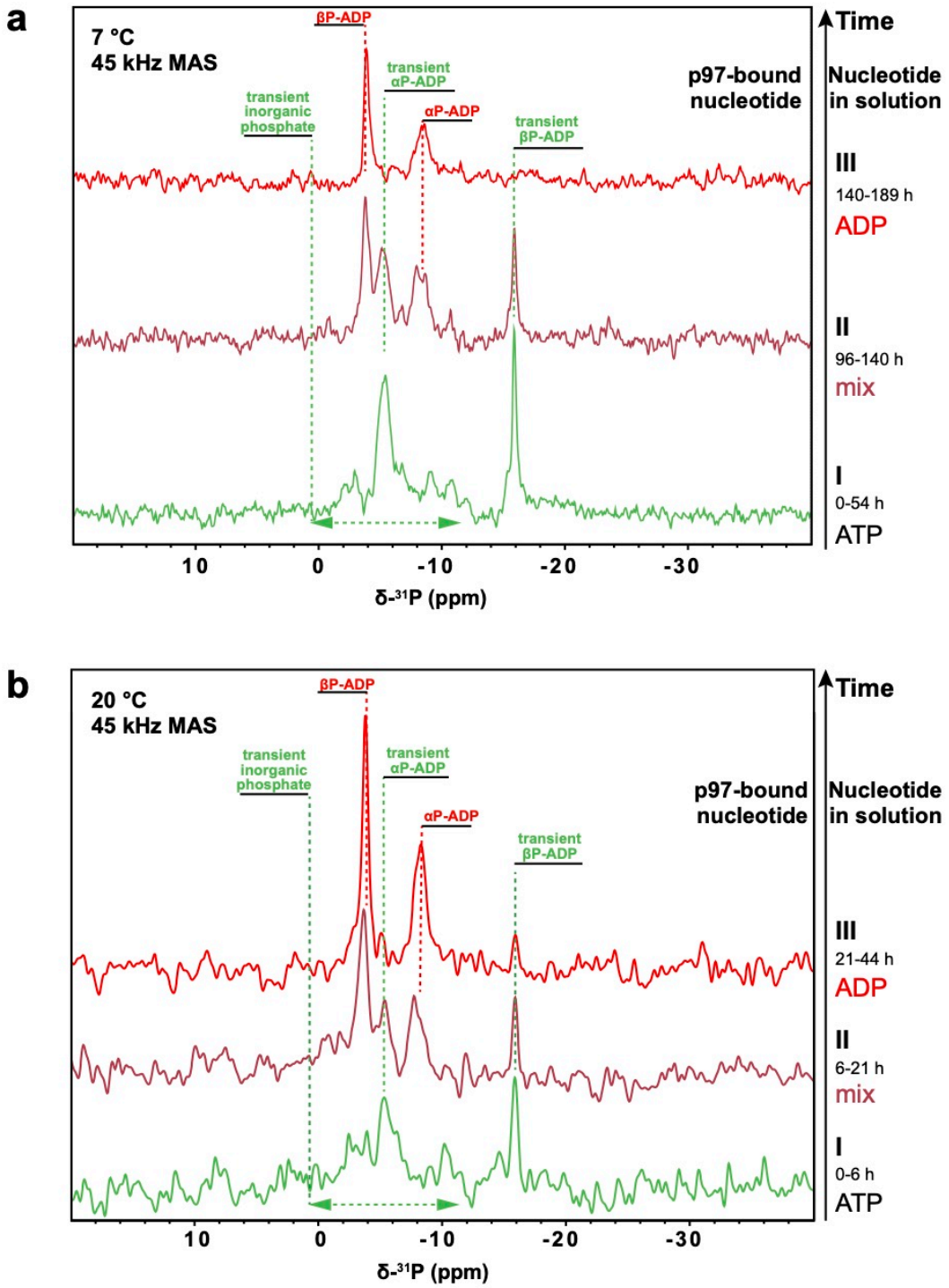

Figure S7. Cross-polarization spectra of nucleotide bound to p97-ND1L during ATP turnover. ^{1}H-^{31}P cross-polarization spectra were recorded in the presence of ATP, a mixture ATP/ADP and finally ADP. Only the nucleotide bound to sedimented p97-ND1L E305Q can be observed in this type of experiment. Sedimented p97 remains in exchange with the free nucleotide reservoir in the surrounding solution, in which the regeneration system initially maintains constant ATP levels. Experiments were performed at 7 °C (**a**) and 20 °C (**b**) with qualitatively similar observations. Due to the increased reaction rate at 20 °C, fewer scans could be acquired and the signal to noise ratio is lower. An overlay of the spectra in Figures S6, S7 confirmed that no signals originating from free nucleotide were detected in the cross-polarization experiments and, vice versa, no signals from bound nucleotide in the directly pulsed experiments.

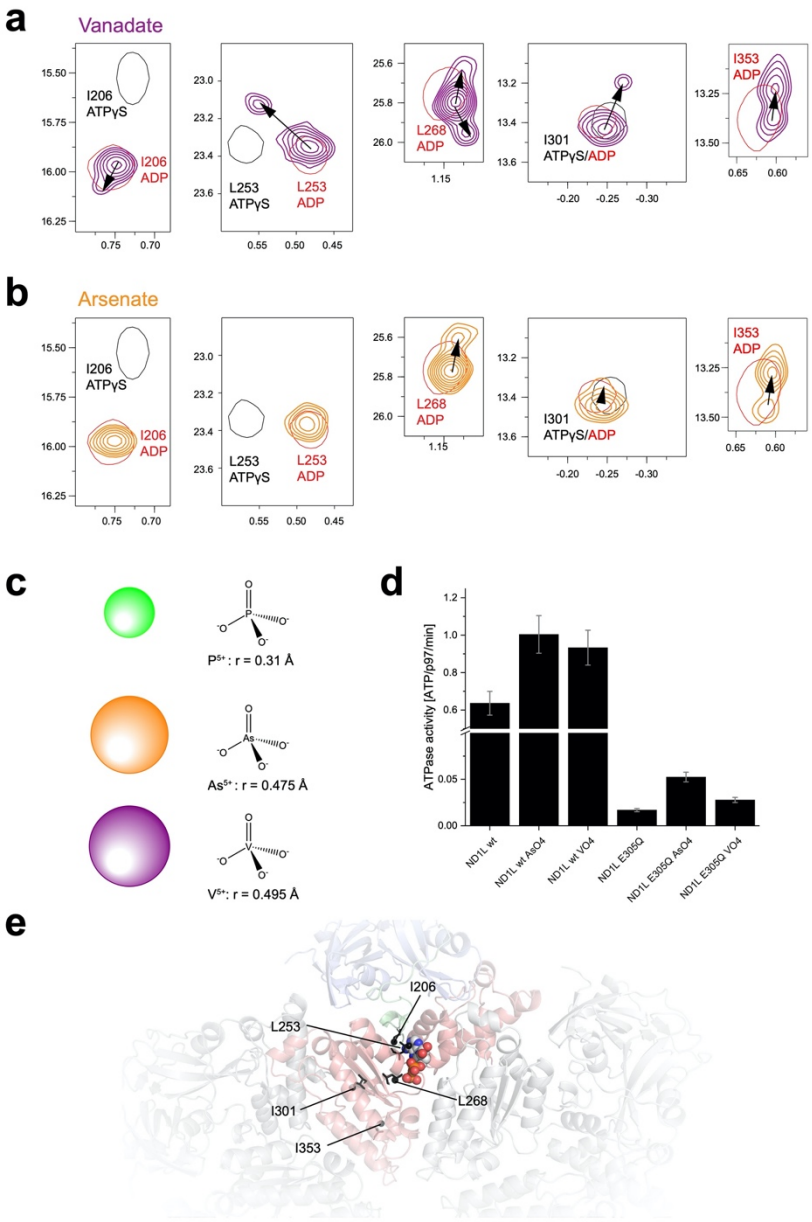

Figure S8. Effect of phosphate-mimicking ions on p97. The effects of phosphate mimics on different ATPase enzymes are not uniform. While arsenate was shown to increase ATPase activity of p97[20], vanadate ions were reported to trap ADP in the nucleotide binding pocket of other AAA+ proteins[15]. **a, b** Superposition of selected correlations from HMQC spectra recorded of p97-ND1L in ADP state after addition of a thousand-fold excess of vanadate (VO_4^{3-}, purple) or arsenate (AsO_4^{3-}, orange), superimposed with reference spectra with ATPγS (black) and ADP (red) bound. The mimics resulted in a splitting of some correlations, more pronounced for vanadate than arsenate. Incomplete trapping by transition state analogues has been noted for other ATPases[21, 22]. **c.** Size comparison of phosphate, arsenate and vanadate ions based on the cation radii[23]. **d.** ATPase activities of p97-ND1L in the presence of 3 mM arsenate/10 mM vandate and p97-ND1L E305Q in the presence of 10 mM arsenate/10 mM vanadate. Here, arsenate exerts a more pronounced effect. **e.** Visualisation of methyl-bearing residues showing chemical shift perturbations upon addition of vanadate on the structure of ADP-bound p97-ND1L (PDB: 1e32). The residues are also listed in Table S2. Even in the presence of more than a thousand-fold excess of free phosphate over protein (200 mM versus 150 µM), no perturbations indicating trapping of ADP-bound p97 in a state reminiscent of the ADP.P_i intermediate were observed (data not shown).

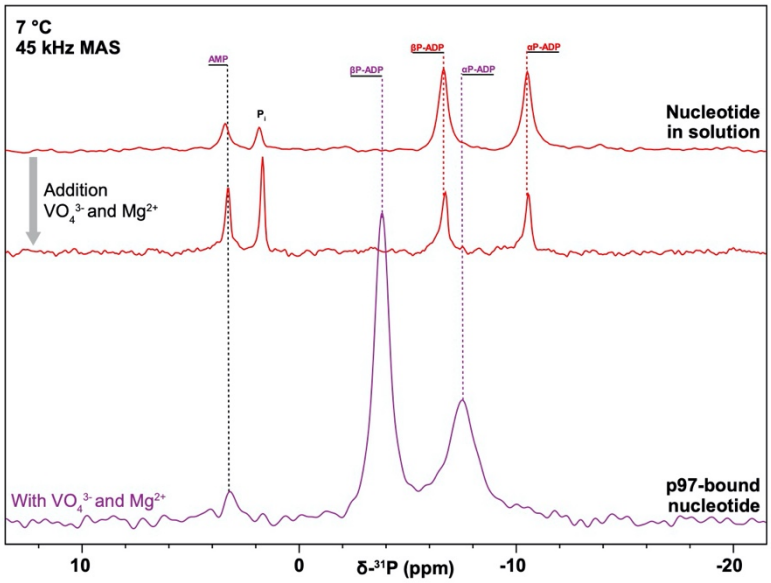

Figure S9. Effect of vanadate ions on bound and free nucleotides. Directly pulsed ^{31}P spectra (red) were recorded of ADP (10 mM) in the absence and presence of vanadate (VO_4^{3-}, 50 mM) and magnesium ($MgCl_2$, 4 mM). ^{1}H-^{31}P cross-polarization spectra (purple) were recorded on sedimented p97-ND1L in the presence of ADP, vanadate and magnesium. The chemical shifts of free ADP are not significantly affected by the presence of vanadate, consistent with previous reports that the formation of anhydrides between vanadate and nucleotides induces no large ^{31}P chemical shift perturbations in the phosphate groups, neither in free solution[24] nor in enzyme-bound complexes[25]. A slow build-up of AMP over time is observed whenever measurements on p97 are performed without regeneration system or once the regeneration system is depleted (compare Figure S6a,b). In the cross-polarization spectra, the two intense signals are assigned to the α- and β-phosphate groups of ADP and display no significant shifts with respect to p97-bound ADP in the absence of vanadate and magnesium. One additional weak signal appears upon vanadate addition. Based on its downfield shift, it is assigned to the phosphate group of AMP. AMP.V, an analogue of ADP[24], binds to p97 unlike AMP itself. In conclusion, the protein-observed NMR spectra from Figure S8 reveal that vanadate ions induce a heterogenous environment inside the binding pocket, evidenced by multiple splittings of methyl group correlations. The nucleotide-observed spectra in this Figure indicate that vanadate ions become trapped predominantly together with ADP and, to a minor extent, AMP.

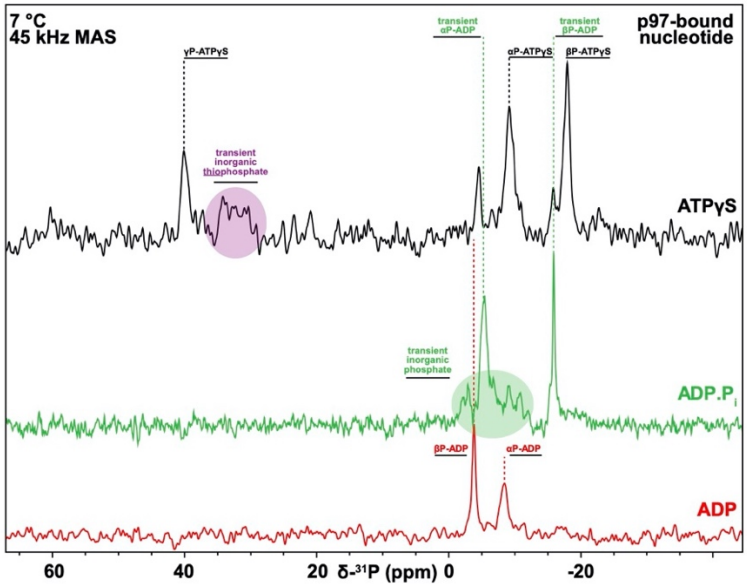

Figure S10. Cross-polarization spectra of ATPγS bound to p97-ND1L. ^{1}H-^{31}P cross-polarization spectra were recorded on sedimented p97-ND1L E305Q in the presence of ATPγS without a regeneration system (black). Only p97-bound nucleotide can be detected in this experiment. The three most intense signals display a pattern of ^{31}P chemical shifts that is characteristic of ATPγS[26, 27] and are thus assigned to its α, β and γ-phosphate groups. Note that thio-substitution of the terminal phosphate induces a large downfield shift. At lower intensity, two additional signals characteristic of the ADP.P_i intermediate are detected (compare with green spectrum), indicating that a small portion of ATPγS undergoes hydrolysis. Cleavage of ATPγS results in inorganic thiophosphate, while cleavage of ATP yields inorganic phosphate. Accordingly, the broad, heterogenous signal assigned to the cleaved γ-phosphate group, highlighted in purple in the black spectrum, is strongly shifted downfield with respect to the signal highlighted in the green spectrum. The fact that this signal shifts entirely upon thio-substitution of the γ-phosphate group proves that it cannot originate from minor populations of ADP or ATP molecules in a different binding pose. We note that for both ATP and ATPγS, the signal of bound (thio)phosphate is shifted upfield by ~5 ppm with respect to the typical resonance from free (thio)phosphate in solution[26]. In the absence of a regeneration system, it cannot be excluded that small amounts of ADP accumulate in the sample over time. A reference spectrum of p97-bound ADP is therefore provided (red). Traces of bound ADP could potentially contribute additional signal intensity to the resonances of the α-phosphate groups of ATPγS and ADP.P_i.

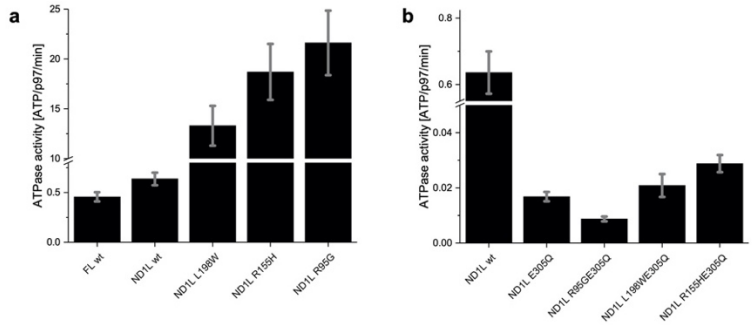

Figure S11. ATPase activities of different p97 constructs and mutants. Turnover rates are given in ATP converted per minute per p97 protomer. Activities were calculated from time derivatives of PEP concentration in the initial regime of the reaction. In this initial regime, the consumption of PEP is approximately linear while ATP and ADP concentrations are constant. Error analysis is described in the Methods.

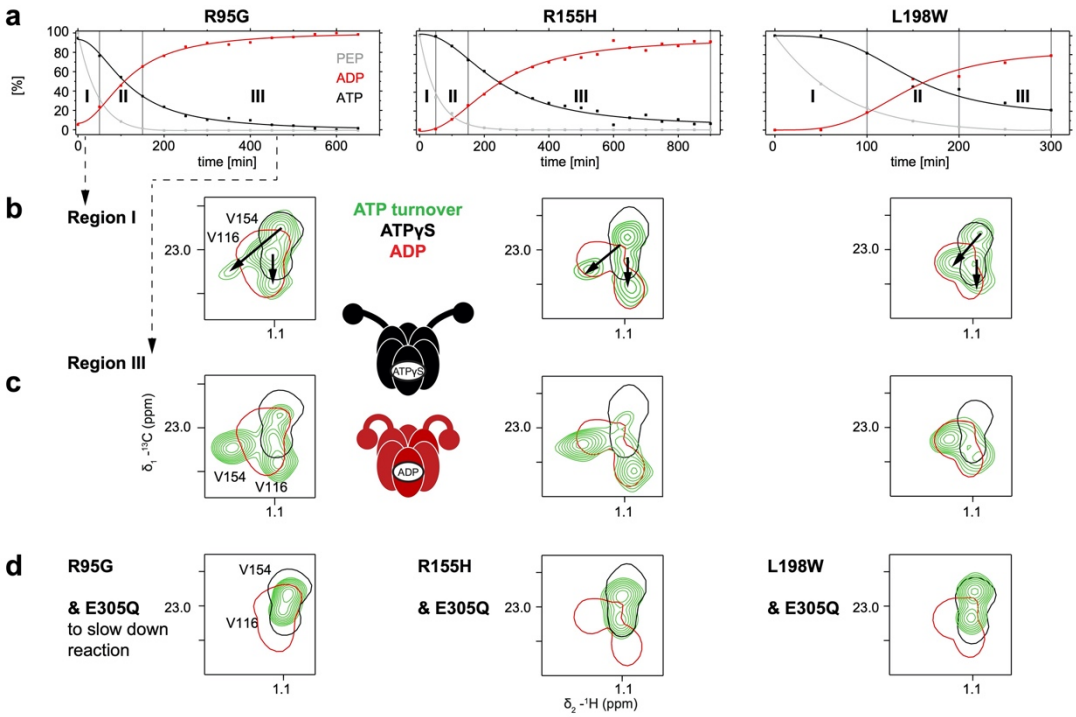

Figure S12. Disease-associated mutants of p97-ND1L during ATP turnover. a. Time course of the ATPase reactions of R95G, R155H and L198W mutants. For wild-type p97, the reaction is inhibited by small amounts of ADP (Figure S4a). In contrast, the disease mutants are not affected by this inhibitory mechanism, and the ATPase reactions proceed swiftly to completion. Methyl correlation spectra of R95G mutant were added up in regions I and III to obtain the spectra shown in green in panel **b** and **c**, respectively. Spectra are superimposed with ATPγS- (black) and ADP-bound (red) reference spectra of each respective mutant. The closeup shown contains residues V154 and V116, which report on the position of the NTD. For all mutants, spectra in region I are similar to the ATPγS-bound reference. Hence, the predominant NTD position is "up" as in the ATPγS-bound reference, whereas in region III the main conformation observed is "down" similar to the ADP-bound reference. **d.** Superposition of spectra of p97-ND1L disease mutants with additional Walker B (E305Q) mutation under ATP turnover with the respective reference spectra. Residues V154 and V116 again serve as probes for the position of the NTD, which is for all three mutants in the "up" conformation as in the ATPγS-bound state. This implies that the pre-hydrolysis step of the reaction cycle has been trapped with ATP.

The disease-associated mutations shift the ADP-bound form of p97 towards a more ATP-like state[1]. The underlying conformational exchange of NTD between up and down positions with respect to D1 domain is fast on the NMR chemical shift time-scale. The fractional populations of NTD in up state are 0.42, 0.14 and 0.27 for R95G, R155H and L198W mutants, respectively. In contrast, the ATPγS-bound form of p97 is little affected by mutation[1]. The reference spectra in black and red contours were recorded on the respective mutants and therefore already account for the partial population shift in ADP-bound p97. In contrast, the complete shift towards the ATPγS-bound form that is observed for all three mutants under ATP turnover in panels b and d is not due to the dynamic domain equilibrium. Rather, it implies that mutant p97 is observed in a pre-hydrolysis state under steady-state conditions. Unlike the domain motion of NTD, the nucleotide exchange that occurs between ADP-, ADP.P_i- and ATP-bound forms of p97 is slow on the chemical shift time-scale. Accordingly, a splitting of correlations rather than a shift is observed in panels b-c.

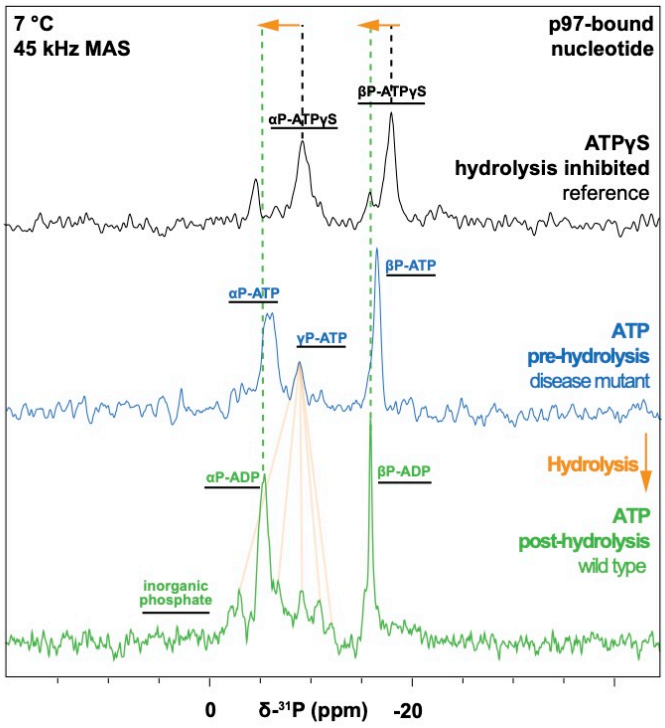

Figure S13. Cross-polarization spectra of nucleotide bound to mutant p97 during ATP turnover. Experiments were performed on sedimented p97-ND1L E305Q with R95G disease-associated mutation in the presence of ATP and a regeneration system. The progression of the ATPase reaction was monitored via directly pulsed ^{31}P spectra to identify the time period during which only ATP was present in solution. The respective cross-polarization spectra were summed up to yield the spectrum shown in blue. The three resonances were assigned to the α, β, γ-phosphate groups of ATP based on the known assignments of ADP.P_i (green, Figure S7) and ATPγS (black, Figure S10) bound to wild-type p97-ND1L E305Q. Notably, the ^{31}P resonances of the α- and β-phosphate groups are progressively shifted downfield as the nucleotide undergoes hydrolysis, from ATPγS over ATP to ADP.P_i. The resonance of the γ-phosphate group is split from one signal in the context of the ATP molecule (pre-hydrolysis, blue) into multiple signals originating from inorganic phosphate (post-hydrolysis, green).

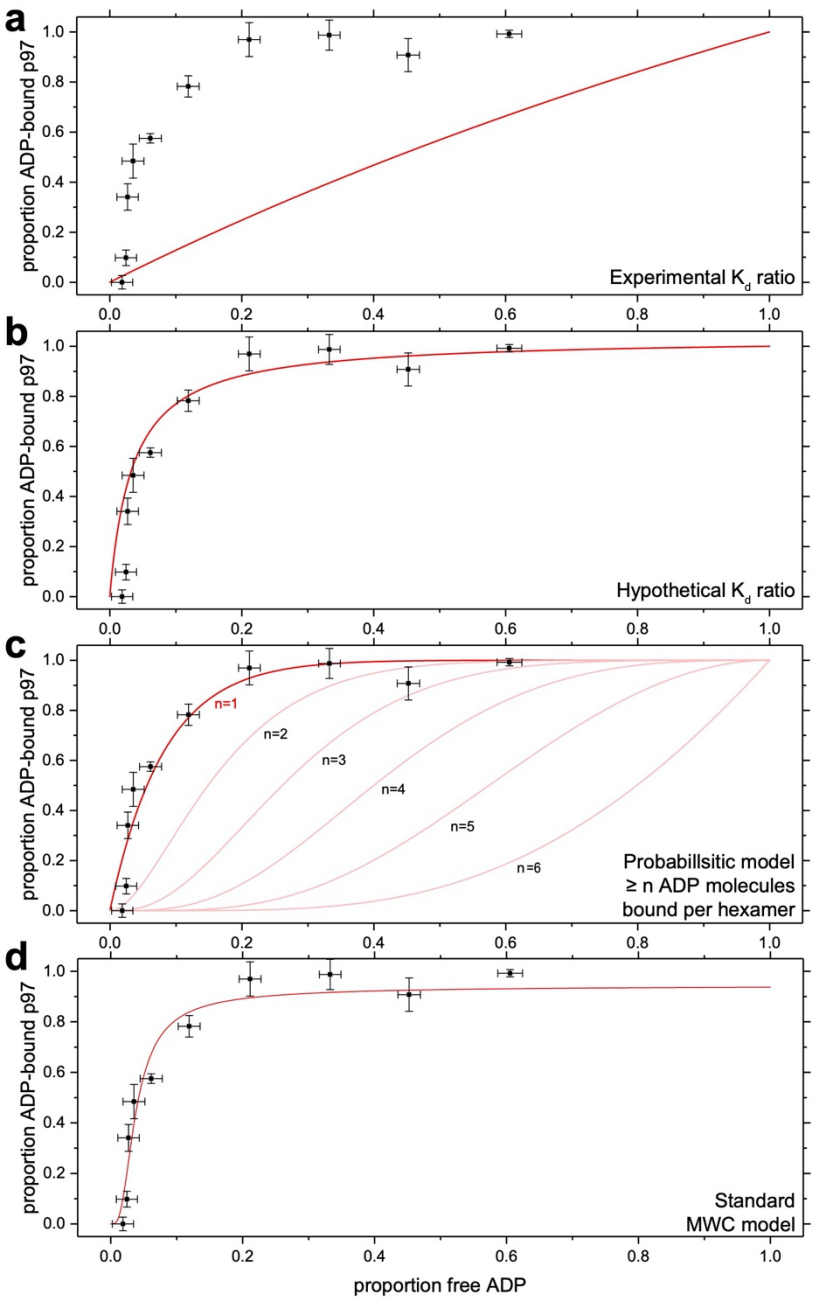

Figure S14. Alternative models for nucleotide binding. The proportions of p97 subunits detected in ADP-bound state are shown as a function of the proportion of free ADP in the reaction mixture. The remaining nucleotide was ATP and the remaining p97 was detected in the ADP.P_i state, which was taken as a proxy for prior ATP binding and hydrolysis. The experimental data points were fitted to different binding models. **a.** Experimentally determined affinities indicate ~1.3-fold tighter binding of ADP over ATP [8, 11, 12] to D1 domain. Non-cooperative binding cannot explain the observed nucleotide occupancies of p97 in the presence of ATP/ADP mixtures. **b.** Only a 30-fold tighter binding of ADP over ATP would explain the experimental data. **c.** The best fit using the probabilistic model reflects well the experimental affinities (Table S3). The prevalence of the ADP-bound state of p97 thus matches the probability of binding at least one ADP per hexamer, implying a scenario whereby a single ADP molecule in the D1 ring 'locks' the entire hexamer. **d.** The data were fitted to the standard MWC model[13], with up-state of NTD equated to T-state and down-state to R-state. This model yields affinities for ADP that are far off the experimental ones. A generalized MWC model considering competitive inhibition by ATP is shown in Figure 4b and shows improved adherence to the experimental affinities for ADP and ATP.

Supporting Tables

Amino acid residue	**ATP-like**	**Disappeared or shifted**	ADP-like
V201	**x**		
I206	**x**		
L213	**x**		
I216			x
I241			x
L243		**x**	
L253		**x**	
I254			x
L268		**x**	
I274		**x**	
L286	**x**		
I301		**x**	
L306	**x**		
V325			x
L328		**x**	
L329		**x**	
M332		**x**	
L335			x
M344		**x**	
I353	**x**		
L357	**x**		
V367			x
I369		**x**	
I371			x
I380		**x**	
I383			x
V407	**x**		
L411		**x**	

Table S1. Chemical shift perturbations detected during ATP turnover. Listed are all residues with an isotope-labelled methyl group (Ile-δ_1, Val-γ_1(*proR*), Leu-δ_1(*proR*), Met-ε_1) within a 20 Å radius around the β-phosphate of the ADP molecule in the crystal structure (PDB: 1e32). They are categorized according to their behaviour under ATP turnover in HMQC spectra of region I (pure ATP, Figures 1b and S3) recorded on p97-ND1L. The spectral appearance is classified into three categories: (*i*) residues with signals different from the ADP-bound reference and shifted towards the correlations of the corresponding ATPγS-bound reference; (*ii*) residues whose correlations disappear or shift in an unknown direction or are shifted to positions other than both references; (*iii*) residues whose signals are similar to the ADP-bound reference throughout the entire ATPase reaction. Residues from the first two categories are displayed on the crystal structure of p97 in Figure 1e.

Residue	Peak splitting with new signal similar to ATPγS-bound p97		Peak splitting		No effect	
	Vanadate	Arsenate	Vanadate	Arsenate	Vanadate	Arsenate
I206			x			x
L253	x					x
L268			x	x		
I301			x	x		
I353	x	x				

Table S2. Chemical shift perturbations detected in the presence of phosphate mimics. Residues that display chemical shift perturbations in spectra of p97-ND1L in ADP-bound state with 50 mM vandate or 50 mM arsenate. The NMR spectra are shown in Figure S8a,b and the location of the residues on the structure is shown in panel e.

	Probabilistic model	Standard MWC model[13]	MWC model with competitive binding[14]	Experimental values (SPR)[8]
$K_{d,ADP}$ [uM]	0.0254	R-state: 19.05 T-state: 290.9	R-state: 0.1487 T-state: 2.131	0.0938
$K_{d,ATP}$ [uM]	0.0524	-	R-state: 1118 T-state: 82.28	0.1236
L [$\cdot 10^5$]	-	7.236	5.386	-
K	2	3	5	-
Adjusted R^2	0.9097	0.9342	0.9099	-
AICc	-40.23	-40.44	-25.66	-
Figure	S14c	S14d	4b	-

Table S3. Comparison of models for coordinated nucleotide binding. The quality criteria of the best fits, AICc and adjusted R^2, along with K, the number of free parameters, are listed. For both MWC models, K_d-values that have an equivalent in experimental affinities are highlighted in red.

	Methyl 2D spectra	Proton 1D spectra
spectrometer ^{1}H frequency [MHz]	800, 900, 950	800, 900, 950
Acquisition		
pulse sequence	^{1}H^{13}C HMQC	directly pulsed ^{1}H with watergate
number of scans	4	128
experiment time	47 min	4 min 25 s
Figures	1c-d S3-5; S8; S12	S2

Table S4. Experimental parameters for solution-state NMR experiments

	Cross polarization	Direct excitation
spectrometer ^{1}H frequency [MHz]	800	800
Rotor outer diameter [mm]	1.3	1.3
MAS [Hz]	45000	45000
Acquisition		
pulse sequence	^{1}H-^{31}P cross polarization with proton decoupling during acquisition	directly pulsed ^{31}P with proton decoupling during acquisition
sweep width [ppm]	154	154
transmitter frequency offset ^{31}P [ppm]	0 (ATP) 31.5 (ATPγS)	0
acquisition time [ms]	41.0	41.0
interscan delay [s]	1	8
number of scans per experiment in time series	8192	256-1024
experiment time	143 min	34-136 min
Figures	2b S7, S9, S10, S13	S6, S9

Table S5. Experimental parameters for solid-state NMR experiments.

Supporting References

1. Schuetz, A. K.; Kay, L. E., A Dynamic molecular basis for malfunction in disease mutants of p97/VCP. *Elife* **2016,** *5*, e20143.
2. Vranken, W. F.; Boucher, W.; Stevens, T. J.; Fogh, R. H.; Pajon, A.; Llinas, M.; Ulrich, E. L.; Markley, J. L.; Ionides, J.; Laue, E. D., The CCPN data model for NMR spectroscopy: development of a software pipeline. *Proteins* **2005,** *59* (4), 687-96.
3. Schrodinger, LLC *The AxPyMOL Molecular Graphics Plugin for Microsoft PowerPoint, Version 1.8*, 2015.
4. Schrodinger, LLC *The JyMOL Molecular Graphics Development Component, Version 1.8*, 2015.
5. Schrodinger, LLC *The PyMOL Molecular Graphics System, Version 1.8*, 2015.
6. Burnham, K. P.; Anderson, D. R.; Huyvaert, K. P., AIC model selection and multimodel inference in behavioral ecology: some background, observations, and comparisons. *Behavioral Ecology and Sociobiology* **2010,** *65* (1), 23-35.
7. Sen, M.; Maillard, R. A.; Nyquist, K.; Rodriguez-Aliaga, P.; Presse, S.; Martin, A.; Bustamante, C., The ClpXP protease unfolds substrates using a constant rate of pulling but different gears. *Cell* **2013,** *155* (3), 636-646.
8. Chou, T. F.; Bulfer, S. L.; Weihi, C. C.; Li, K. L.; Lis, L. G.; Walters, M. A.; Schoenen, F. J.; Lin, H. J.; Deshaies, R. J.; Arkin, M. R., Specific Inhibition of p97/VCP ATPase and Kinetic Analysis Demonstrate Interaction between D1 and D2 ATPase Domains. *Journal of Molecular Biology* **2014,** *426* (15), 2886-2899.
9. Tang, W. K.; Li, D.; Li, C. C.; Esser, L.; Dai, R.; Guo, L.; Xia, D., A novel ATP-dependent conformation in p97 N-D1 fragment revealed by crystal structures of disease-related mutants. *EMBO J* **2010,** *29* (13), 2217-29.
10. HILL, A. V., The possible effects of the aggregation of the molecules of haemoglobin on its dissociation curves. *J Physiol (Lond)* **1910,** *40*, 4-7.
11. Bulfer, S. L.; Chou, T. F.; Arkin, M. R., p97 Disease Mutations Modulate Nucleotide-Induced Conformation to Alter Protein-Protein Interactions. *ACS Chem Biol* **2016,** *11* (8), 2112-6.
12. Tang, W. K.; Xia, D., Altered Intersubunit Communication Is the Molecular Basis for Functional Defects of Pathogenic p97 Mutants. *Journal of Biological Chemistry* **2013,** *288* (51), 36624-36635.
13. Monod, J.; Wyman, J.; Changeux, J. P., On the Nature of Allosteric Transitions: A Plausible Model. *J Mol Biol* **1965,** *12* (1), 88-118.
14. Najdi, T. S.; Yang, C.-R.; Shapiro, B. E.; Hatfield, G. W.; Mjolsness, E. D., Application of a generalized MWC model for the mathematical simulation of metabolic pathways regulated by allosteric enzymes. *Journal of bioinformatics and computational biology* **2006,** *4* (2), 335-355.
15. Rodriguez-Aliaga, P.; Ramirez, L.; Kim, F.; Bustamante, C.; Martin, A., Substrate-translocating loops regulate mechanochemical coupling and power production in AAA+ protease ClpXP. *Nat Struct Mol Biol* **2016,** *23* (11), 974-981.
16. Henn, A.; Cao, W.; Hackney, D. D.; De La Cruz, E. M., The ATPase cycle mechanism of the DEAD-box rRNA helicase, DbpA. *J Mol Biol* **2008,** *377* (1), 193-205.
17. Lewis, J. H.; Lin, T.; Hokanson, D. E.; Ostap, E. M., Temperature dependence of nucleotide association and kinetic characterization of myo1b. *Biochemistry* **2006,** *45* (38), 11589-11597.
18. Robblee, J. P.; Cao, W.; Henn, A.; Hannemann, D. E.; De La Cruz, E. M., Thermodynamics of nucleotide binding to actomyosin V and VI: a positive heat capacity change accompanies strong ADP binding. *Biochemistry* **2005,** *44* (30), 10238-10249.
19. Wendler, P.; Ciniawsky, S.; Kock, M.; Kube, S., Structure and function of the AAA+ nucleotide binding pocket. *Biochim Biophys Acta* **2012,** *1823* (1), 2-14.
20. Tillotson, J.; Zerio, C. J.; Harder, B.; Ambrose, A. J.; Jung, K. S.; Kang, M.; Zhang, D. D.; Chapman, E., Arsenic Compromises Both p97 and Proteasome Functions. *Chem Res Toxicol* **2017,** *30* (7), 1508-1514.
21. Kaur, H.; Abreu, B.; Akhmetzyanov, D.; Lakatos-Karoly, A.; Soares, C. M.; Prisner, T.; Glaubitz, C., Unexplored Nucleotide Binding Modes for the ABC Exporter MsbA. *J Am Chem Soc* **2018,** *140* (43), 14112-14125.

22. Wiegand, T.; Cadalbert, R.; Lacabanne, D.; Timmins, J.; Terradot, L.; Bockmann, A.; Meier, B. H., The conformational changes coupling ATP hydrolysis and translocation in a bacterial DnaB helicase. *Nat Commun* **2019,** *10* (1), 31.
23. Holleman, A. F.; Wiberg, E.; Wiberg, N., Lehrbuch der anorganischen Chemie. 102., stark umgearb. u. verb. Aufl. ed.; de Gruyter: Berlin u.a., 2007.
24. Geraldes, C. F.; Castro, M. M., Multinuclear NMR study of the interaction of vanadate with mononucleotides, ADP, and ATP. *Journal of inorganic biochemistry* **1989,** *37* (3), 213-232.
25. Ray, B. D.; Rao, B. D. N.; Moore, J. M., 31P NMR studies of enzyme-bound substrate complexes of yeast 3-phosphoglycerate kinase: III. Two ADP binding sites and their Mg(II) affinity; effects of vanadate and arsenate on enzymic complexes with ADP and 3-P-glycerate. *Journal of inorganic biochemistry* **1990,** *40* (1), 47-57.
26. Jaffe, E. K.; Cohn, M., 31P nuclear magnetic resonance spectra of the thiophosphate analogues of adenine nucleotides; effects of pH and Mg2+ binding. *Biochemistry* **1978,** *17* (4), 652-7.
27. Ullrich, S. J.; Hellmich, U. A.; Ullrich, S.; Glaubitz, C., Interfacial enzyme kinetics of a membrane bound kinase analyzed by real-time MAS-NMR. *Nature Chemical Biology* **2011,** *7* (5), 263-270.